JOURNAL OF AIRCRAFT
Vol. 32, No. 3, May–June 1995

In-Flight Pressure Measurements on a Subsonic Transport High-Lift Wing Section

Long P. Yip*
NASA Langley Research Center, Hampton, Virginia 23681
Paul M. H. W. Vijgen†
High Technology Corporation, Hampton, Virginia 23666
Jay D. Hardin‡
Lockheed Engineering and Sciences Company, Inc., Hampton, Virginia 23666
and
C. P. van Dam§
University of California, Davis, Davis, California 95616

The NASA Langley Transport Systems Research Vehicle (B737-100 aircraft) was used to obtain in-flight flow characteristics including surface pressures and surface shear stresses for a full-chord wing section, including the slat, main-wing, and triple-slotted, Fowler-flap elements. Chordwise pressure distributions were obtained at the 58% semispan station using thin pressure belts. Flow characteristics observed in the chordwise pressure distributions included leading-edge regions of high-subsonic flows, leading-edge attachment-line locations, slat and main-wing cove-flow separation and reattachment, and trailing-edge flow separation. In addition, surface shear-stress measurements were made using Preston-tube probes on each element. Computational analysis of the in-flight pressure measurements using two-dimensional, viscous-flow, multielement methods and simple-sweep theory showed reasonable agreement. However, overprediction of the suction pressures on the flap elements indicates a need for more detailed (off-surface) measurements of the flow and the in-flight flap geometry to aid modeling of the complex three-dimensional flowfield.

Nomenclature

b = wingspan, 93.0 ft
C_f^* = skin-friction coefficient (also see discussion in Description of Flight Experiment), τ/q_∞
C_L = aircraft lift coefficient, lift/$(q_\infty S)$
C_p = pressure coefficient
$\bar{c}$ = mean aerodynamic chord, 11.20 ft
h = pressure altitude, ft
M = freestream Mach number
q_∞ = freestream dynamic pressure, psf
$R_{\bar{c}}$ = Reynolds number based on true airspeed and $\bar{c}$
S = reference wing area, 980 ft^2
V_i = indicated airspeed, kt
x/c = non dimensional chordwise coordinate
α = aircraft angle of attack, deg
δ_f = flap deflection, deg
η = nondimensional semispan location, $2y/b$
Λ_{LE} = leading-edge sweep angle, deg
τ = surface shear stress computed from Preston-tube measurements, psf

Received Dec. 5, 1993; revision received June 24, 1994; accepted for publication Sept. 15, 1994.

*Research Engineer, Vehicle Performance Branch, Flight Dynamics and Control Division. Senior Member AIAA.
†Research Scientist; currently Senior Specialist Engineer, HSCT Aerodynamics, Boeing Commercial Airplane Group, Seattle, WA 98124. Member AIAA.
‡Research Engineer. Member AIAA.
§Associate Professor, Department of Mechanical and Aeronautical Engineering. Senior Member AIAA.

Introduction

HIGH-LIFT system aerodynamics can significantly impact the overall design of transport aircraft in terms of sizing, performance, system complexity, and noise and safety certification.[1] Currently, the improved design of subsonic high-lift systems remains a technical challenge mostly due to the limited understanding of the complex flow physics associated with high-lift flows. Multielement, high-lift flows are sensitive to Reynolds and Mach number effects; and therefore, the aerodynamic performance of three-dimensional high-lift systems is generally difficult to extrapolate from wind-tunnel or to predict in computational fluid dynamics (CFD) studies. In order to improve the design methodology for high-lift systems, additional experimental data with sufficient flow details on transport-type swept wings are needed at actual flight Reynolds and Mach numbers to better understand high-lift flows. Thus far, only a very limited number of flight investigations have been conducted with sufficiently detailed flow measurements on a high-lift system for correlation with ground-based investigations and to guide three-dimensional CFD modeling. One such investigation was reported by Greff[2] on an Airbus A310-300 aircraft with flow measurements concentrated in the slat region.

As part of a multiphased research program at NASA Langley, flight tests are being conducted on the Transport Systems Research Vehicle (TSRV), a B737-100 aircraft, to obtain detailed full-scale flow measurements on a multielement high-lift system at various flight conditions. The purpose of this article is to report the initial flight-test results, including flow visualizations, surface pressure distributions, and surface shear-stress measurements. Before describing the flight experiment and its results, a brief background on aspects of multielement high-lift flows relevant to the data included is presented.

Multielement Flow Issues

The flowfield around a multielement transport wing with sweep is characterized by several aerodynamic phenomena that are generally highly interrelated, complex in nature, and not fully understood. Accurate prediction of surface-pressure distributions, merging shear layers, and separated-flow regions over multielement airfoils is an essential requirement in the design of advanced high-lift systems for efficient subsonic transport aircraft. The availability of detailed measurements of pressure distributions and boundary-layer flow parameters at flight Reynolds and Mach numbers is critical to the development and evaluation of CFD methods for high lift.[3,4] Detailed measurements and analysis of the multielement flowfield have generally been limited to two-dimensional studies. Previous detailed flow measurements in the wind-tunnel investigations have included Reynolds-stress components, however, at subscale Reynolds numbers and only in two dimensions.[5-8] These results have been applied towards the development and validation of two-dimensional multielement numerical codes. Two-dimensional multielement flow issues include 1) compressibility effects including shock/boundary-layer interaction on the slat, 2) laminar separation-induced transition along the upper surfaces, 3) confluent turbulent boundary layer(s) [the merging of wake(s) from upstream elements with the boundary layers of downstream elements], 4) cove separation and reattachment, and 5) flow separation on the flap upper surfaces and the main element.

Availability of detailed flow data in three dimensions at full-scale (flight) Reynolds numbers has been much more limited. To contribute to the understanding and correlation of high-lift research between wind tunnel, CFD, and flight, experiments are needed for three-dimensional swept wings at full-scale Reynolds numbers. Further understanding of scale effects is required to accurately extrapolate subscale, three-dimensional results to full-scale, flight conditions.[9-11]

Three-dimensional multielement flow issues include 1) leading-edge transition and relaminarization; 2) sweep effects on confluent boundary-layer development, turbulent boundary-layer separation, and separated cove flows; 3) highly three-dimensional, local flow modifications; e.g., vortex generators; flap side-edge-separated flows and tip effects; and flow interactions with slat brackets and flap-track fairings, engine pylons, and landing-gear struts. The three-dimensional multielement issues of leading-edge attachment-line transition and the potential for relaminarization are discussed in more detail in the following section.

Attachment-Line Transition and Relaminarization Issues

In three-dimensional, swept-wing flows, the flow along the attachment line (a locus of points near the leading-edge dividing upper- and lower-surface flows) can be laminar, transitional, or turbulent, depending on the pressure distribution, the leading-edge sweep angle, and the Reynolds number.[12-14] If attachment-line transition occurs, the resulting changes in the development of boundary-layer flows can significantly influence the downstream turbulent flowfield. Relaminarization of the flow downstream of a turbulent attachment line can occur if the streamwise flow acceleration is sufficiently strong.[15-17] If the flow ahead of a steep adverse pressure gradient along the upper surface of the elements is laminar, an additional Reynolds number effect can occur due to the presence of a laminar-separation bubble and its effect on subsequent turbulent-flow behavior.

The issues of leading-edge transition and relaminarization, illustrated in Fig. 1 for a smooth, single-element, swept wing, are important in the extrapolation of subscale, three-dimensional wind-tunnel results to flight. Typically, three-dimensional wind-tunnel data used to extrapolate maximum lift in flight are obtained at Reynolds numbers where wing stall is dominated by conventional scale effects.[18] Conventional scale effects refer to the increase of maximum lift with Reynolds number due to the thinning of the turbulent boundary layer in the wing trailing-edge region and the subsequent aft movement of the trailing-edge flow separation point. At flight Reynolds numbers, attachment-line transition can occur causing turbulent flow to start from the attachment line. By shifting forward the starting point of the turbulent boundary layer, the trailing-edge separation location can also shift forward due to the increased growth of the turbulent boundary layer. Because of the increased extent of trailing-edge separation, a significant reduction in lift can occur. However, because of steep favorable pressure gradients associated with high-lift flows, relaminarization is possible for some sections of the wing and would thereby alleviate some of the lift loss expected as a result of the attachment-line transition. In a high Reynolds number wind-tunnel investigation of a swept-wing configuration without slats, maximum-lift losses of the order of 15% have been measured when transition occurred along the attachment line and relaminarization did not occur.[10]

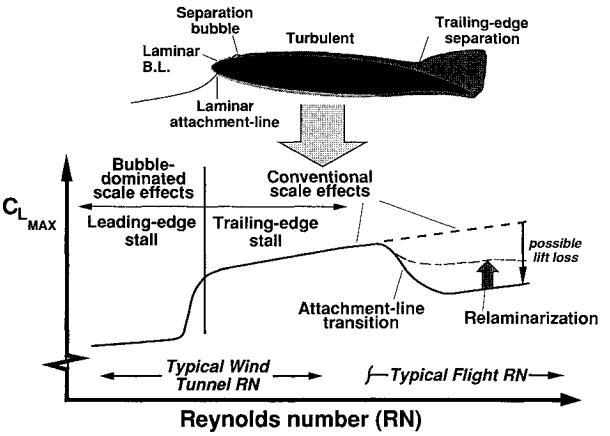

Fig. 1 Effect of attachment-line transition and relaminarization on maximum lift of swept single-element wing.

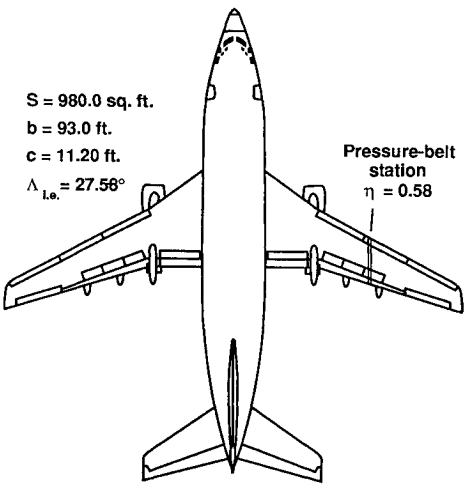

Fig. 2 Planform view of the B737-100 aircraft.

Description of Flight Experiment

The NASA Langley TSRV was the prototype aircraft used in the development of the Boeing B737-100 and has been significantly modified for flight systems research.[19] In its unmodified state, the Boeing 737-100 is a twin-jet, short-haul, subsonic transport designed to carry approximately 100 passengers with a cruise speed of Mach 0.78. In order to obtain short-field takeoff and landing performance the aircraft incorporates leading-edge devices and a triple-slotted flap system. Figure 2 shows a planform view of the B737-100 configuration and illustrates the overall geometric characteristics.

Inboard leading-edge Krüger flaps (not indicated in Fig. 2) and outboard leading-edge slats are extended in conjunction with the triple-slotted trailing-edge flaps. As shown in Fig. 3, the outboard high-lift wing section studied in this aricle consists of five elements: 1) the leading-edge slat, 2) the main wing with fixed leading edge, 3) the fore flap, 4) the midflap, and 5) the aft flap. At flap settings over 25 deg the two most outboard slat segments are fully extended and deflected an additional increment (see Fig. 3), effectively creating a break in the leading edge between the inboard slat and outboard slats (see Figs. 4 and 5a). At the lower flap settings, only a very small slot exists between the slat and main-wing elements (see Fig. 3).

Instrumentation for the full-chord, wing-section measurements is illustrated in Fig. 4. Surface pressure distributions, Preston-tube skin-friction measurements, and flow-visualization results were obtained on the starboard wing of the research aircraft. The chordwise pressure distributions were measured at a nominal spanwise station of $\eta = 0.58$ on the upper and lower surfaces of the slat, main-wing, and flap elements using thin belts of plastic tubing (0.062 in. o.d./0.028 in. i.d.), which were wrapped around each element. The belts were attached to the surface with thin (0.005 in.) adhesive tape. To minimize belt edge effects, five extra (nonfunctioning) tubes were added to each side, and the sides of each belt were ramped with a silicon-rubber compound. The spacing of the pressure orifices was reduced in the leading-edge regions in order to be able to capture the leading-edge suction peaks. The technique of using external pressure belts has been commonly used in previous flight studies and was shown to generally provide good surface pressure measurements when compared to flush surface orifices.[20]

A total of 160 pressure tubes (144 for pressure distributions, 12 for static and total measurements of the Preston tubes, and 4 spare tubes) were connected to five electronically scanning pressure (ESP) modules that were located in the wing cove region (see Fig. 4). The ESP modules were maintained at a constant temperature to minimize zero shift of the measurement, and two differential-pressure transducer ranges (2.5 and 5.0 psi) allowed high resolution of the pressure data. A plenum chamber was housed in the wing cove region to provide the reference pressure for the ESP transducers; the reference pressure was monitored with an absolute pressure gauge and was related to the static pressure measured by the aircraft pitot-static probe. A small data-acquisition unit was located in the outboard flap track fairing of the wing (see Fig. 4) to access and address the ESP transducers. The digital output data were processed by an on-board computer for real-time graphical display and stored on an optical disk for postflight data analysis. Pressures were recorded at a rate of 10 samples/s while aircraft flight parameters were recorded at a rate of 20 samples/s. The pneumatic lag for the longest tube length was measured in ground tests and determined to be approximately 0.5 s, and was taken into account in the measurement and reduction of data.

In order to provide corrections of the static pressure due to probe position error for each flap setting, an airspeed calibration flight was conducted prior to the research flights using a tracking-radar method.[21] These corrections along with temperature measurements were used to compute freestream static

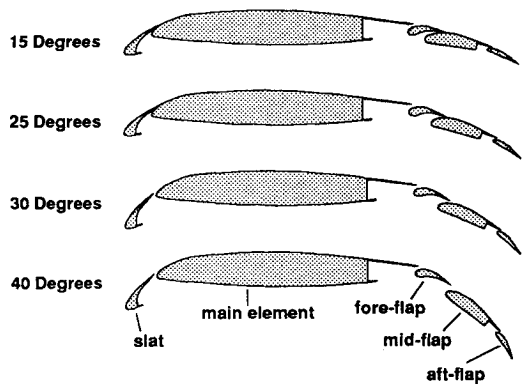

Fig. 3 Wing sections at various flap settings (outboard wing).

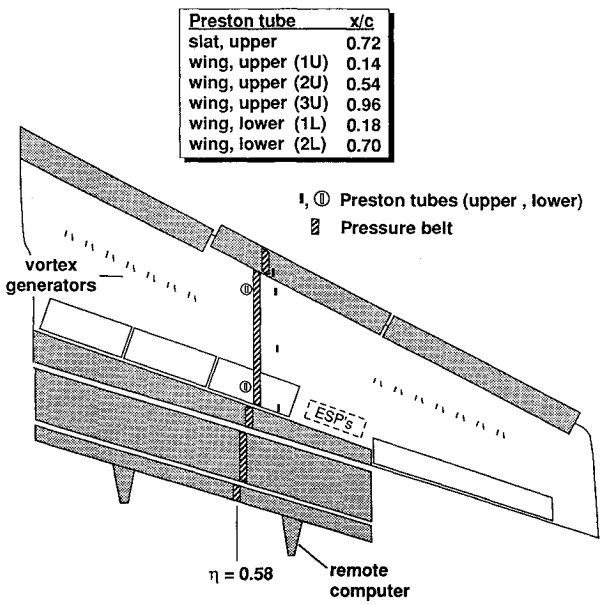

Fig. 4 Instrumentation layout.

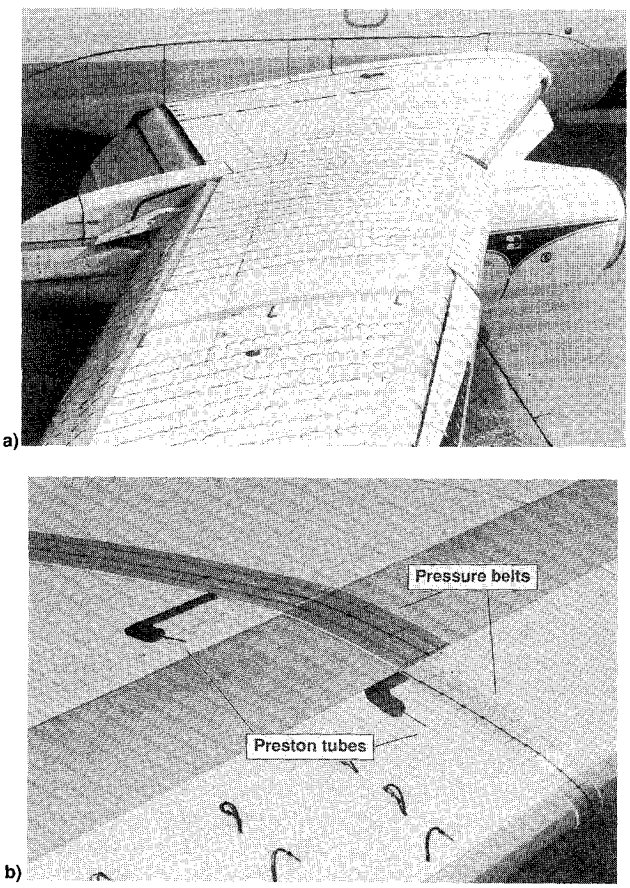

Fig. 5 Pressure-belt and Preston-tube installation: a) B-737 subsonic high-lift flight experiment, wing-section pressures and flow visualization ($\delta_f = 40$ deg) and b) pressure-belt and Preston-tube installation, leading-edge slat and main wing element (close-up view, $\delta_f = 15$ deg).

and dynamic pressures as well as Mach and Reynolds numbers. Also, angle-of-attack corrections were obtained for each flap setting by calibrating the aircraft angle-of-attack vane against pitch attitude obtained from the aircraft inertial navigation system in steady level flight. Lift coefficients were determined from steady, 1-g flight maneuvers using aircraft weight calculated from aircraft fuel consumption measured by fuel-flow sensors. Thrust corrections obtained from a standard engine performance deck were applied to remove the thrust contribution from the lift data.

Flow visualization was obtained by applying nylon yarn tufts to the upper surfaces of the outboard flap and the main-wing elements (see Fig. 5) to indicate local regions of flow separation. The tuft patterns were recorded with still and video photography to allow for postflight analysis and correlation.

Preston tubes were installed on the upper and lower surfaces of the main-wing element, and one Preston tube was installed on the slat upper surface (see Figs. 4 and 5). The Preston-tube probes were installed in the freestream direction just outboard of the pressure belt and staggered spanwise to minimize interference effects of the probes on each other. These probes contain a flush orifice in addition to the pitot pressure orifice to measure static and total pressures within the boundary layer, and the local skin friction coefficient can be determined based on the measured pressure differential at the tube.[22] The o.d. of the modified Preston tube used here were 0.083 in. for the wing locations and 0.042 in. for the slat location. The calibration expression for these probes is valid if both the static and the total port are located within the law-of-the-wall region of the turbulent boundary layer.[22] Since the boundary-layer state, its thickness as well as its orientation are dependent on the flap setting and the various flight parameters, skin-friction values based on the Preston-tube measurements are listed in this paper as C_f^*; where the superscript indicates that these measurements do not necessarily reflect actual skin-friction values if the Preston-tube readings were outside the valid calibration range, e.g., if the flow was laminar. Preston-tube measurements on the flap elements were obtained without the instrumentation installed on the wing and the slat during a different phase of the flight experiment.[23]

Flight-Test Results

The flight experiments covered a range of Reynolds and Mach numbers as the aircraft was flown at pressure altitudes of 5, 10, 15, and 20 kft. The Reynolds number based on the mean aerodynamic chord $R_{\bar{c}}$ (where the mean aerodynamic chord $\bar{c}$ = 11.20 ft) ranged from 1.0×10^6 to 2.1×10^6, and the freestream Mach number varied from 0.16 to 0.40. Test conditions and test points obtained in flight with flap deflections of 15, 25, 30, and 40 deg are shown in Fig. 6, as well as lines of constant Reynolds and Mach numbers for standard atmospheric conditions. As indicated by Fig. 6, flight at increasing altitudes provides conditions of increasing Mach number and decreasing Reynolds number for a given indicated airspeed V_i, which corresponds approximately to a constant lift coefficient for a given aircraft weight.

The flight-test points were obtained for each of the flap settings at 1-g, steady conditions in level flight with the aircraft initially flown at a high nominal airspeed and then slowed to the stick-shaker speed. Data were sampled for approximately 30 s at each constant-airspeed test point. In addition, data were recorded during the deceleration of the aircraft between selected test points. The aircraft was decelerated at a nominal rate of 1 kt/5 s while constant altitude was maintained. Pertinent test points were repeated to ensure data repeatability. All data were obtained with the landing gear retracted. The research flight deck on the TSRV allowed autothrottle and autopilot operations of the aircraft for constant airspeed and altitude modes of testing.

The results presented here are for a flight altitude of 10 kft unless otherwise noted. The surface static pressure measurements at this altitude are representative for results obtained at the other altitudes.

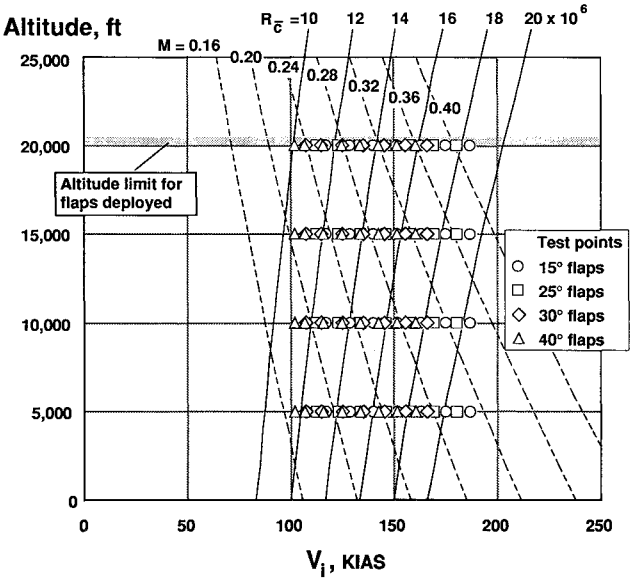

Fig. 6 Flight-test conditions.

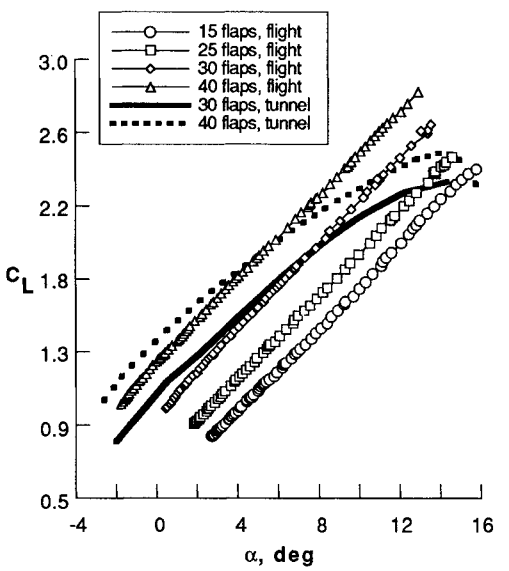

Fig. 7 Comparison of trimmed data from flight and low Reynolds number ($R_{\bar{c}}$ = 1.4 × 10^6) wind-tunnel data (thrust contribution removed). In flight, $R_{\bar{c}}$ ranged from 1.04 × 10^7 at C_L = 2.76 and δ_f = 40 deg to 2.03 × 10^7 at C_L = 0.86 and δ_f = 15 deg.

Trimmed-Lift Data

Trimmed-lift coefficients from representative flight data are shown in Fig. 7 for the TSRV configuration with flap deflections of 15, 25, 30, and 40 deg. For the angle-of-attack range tested, the lift curves remained nearly linear with no significant slope changes except for a slight decrease in the lift-curve slope for the 15-deg-flap case at high angles of attack. In Fig. 7, the flight lift data are also compared with available wind-tunnel lift data[24] for the 30- and 40-deg-flap settings. The wind-tunnel investigation used a one-eighth scale model of the TSRV with flow-through nacelles. The wind-tunnel data were obtained at test conditions of M = 0.14 and $R_{\bar{c}}$ = 1.4 × 10^6, significantly less than the flight Reynolds numbers that ranged from $R_{\bar{c}}$ = 1.04 × 10^7 at low-speed conditions (C_L = 2.76, δ_f = 40 deg) to 2.03 × 10^7 at high-speed conditions (C_L = 0.86, δ_f = 15 deg). Wind-tunnel force and moment data were recomputed for 18% $\bar{c}$, the nominal c.g. location in flight, and trimmed-lift coefficients were estimated based

on stabilizer requirements for trimmed flight. The comparison shows significant differences between flight and wind-tunnel data, likely due to the discrepancy in the Reynolds numbers as well as differences in aeroelastic deformations of the high-lift elements between the wind-tunnel model and the actual airframe. At high angles of attack, the underprediction in the wind-tunnel data is probably due to premature flow separation at the much lower wind-tunnel Reynolds number conditions. At low angles of attack, the overprediction in the wind-tunnel data may be a result of an inverse Reynolds number effect on multielement airfoils where lift decreases with increasing Reynolds number for given geometry.[18,25]

Pressure Distributions and Skin-Friction Measurements

Pressure distributions measured for all elements on the TSRV, high-lift wing section are presented in Fig. 8 for the 15- and 40-deg-flap settings. Several observations can be made based on the overall flight-measured pressure distributions:

1) Changing the angle of attack affected primarily slat and main-wing pressure loading, and had little effect on the flap pressures. The small variance of flap loading with angle of attack is explained by the fixed deflection geometry of the upstream element that largely determines the in-flow angle for the flap element.

2) Because of sweep effects, maximum C_p values were less than the two-dimensional value for the stagnation point. Also,

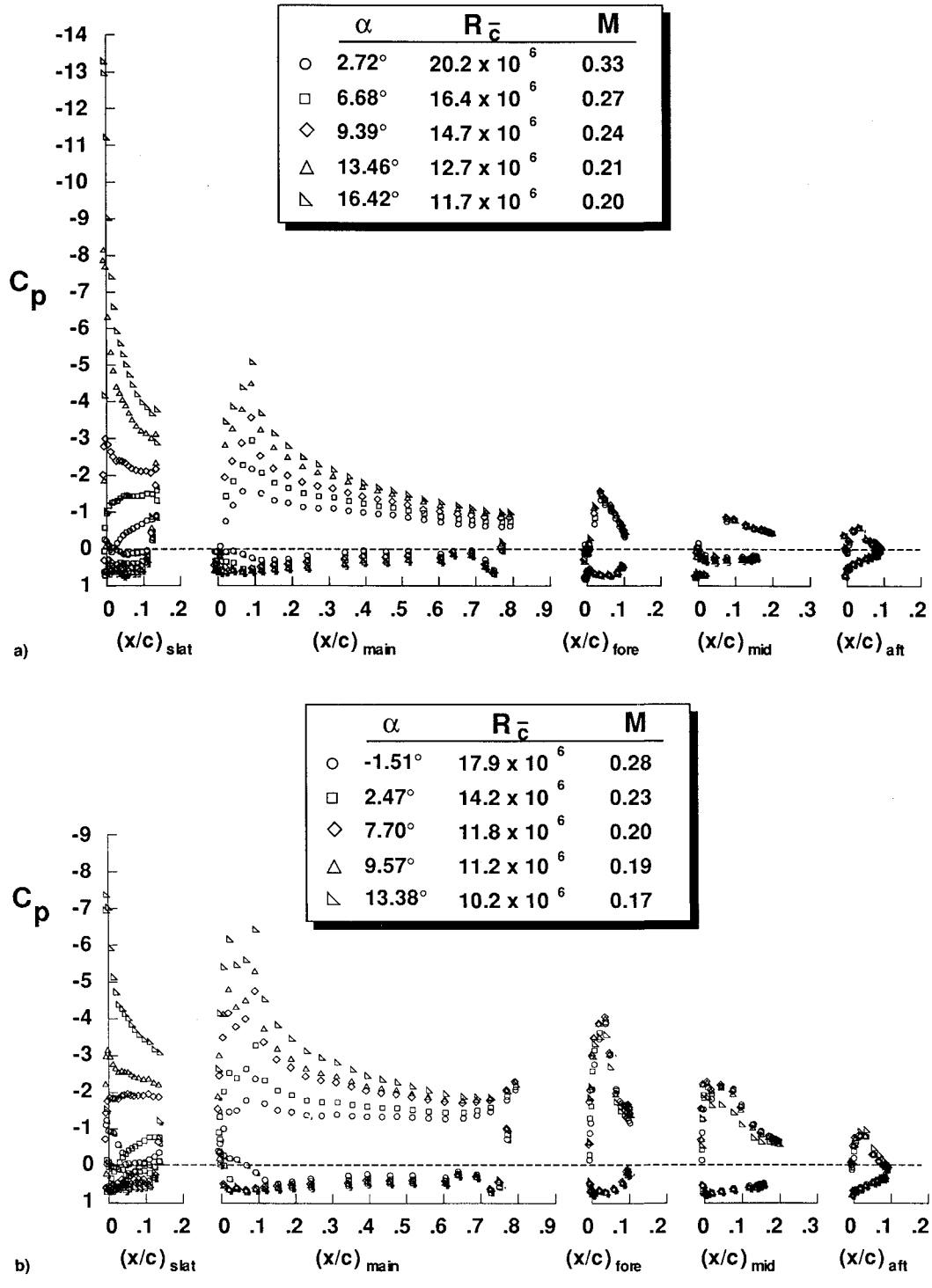

Fig. 8 Wing-section pressure distributions (η = 0.58). δ_f = a) 15 and b) 40 deg.

flow reattachment in the main-wing cove is indicated by the near-maximum C_p values.

3) Pressures at the trailing edge of each element, except for the aft flap, do not recover completely due to the influence of the downstream element. The accelerating flow region between the elements also causes changes in the trailing-edge pressure distributions, e.g., note the decreasing main-wing element upper-surface pressures near the trailing edge with increasing flap deflection. The higher velocities near the trailing edge also relieve the pressure rise on the leading edge of the downstream element, thus alleviating potential separation problems that could cause loss in lift. These multielement flow phenomena are attributed to the "circulation effect" and "dumping effect" as described by Smith.[26]

Flow characteristics of the individual elements of the high-lift system are examined in more detail in the following sections. More detailed plots of the pressure distributions of the individual elements are presented in Ref. 28.

Slat-Element Flow Characteristics

A comparison of the slat pressure distributions for the 15- and 40-deg-flap setting (Fig. 8) shows similar results for a given angle of attack (e.g., note the pressure distributions at $\alpha \approx 2.5$, 9.5, and 13.5 deg). Both flap settings show favorable upper-surface pressure gradients at low angles of attack, nearly flat pressure distributions at moderate angles of attack, and an upper-surface suction peak near the leading edge with a subsequent adverse gradient downstream at high angles of attack. For the 15-deg-flap setting, the upper-surface suction peak reached a minimum value of $C_p = -13.18$ at the highest available angle of attack, $\alpha = 16.42$ deg, and a freestream Mach number of 0.20. This C_p value corresponds to a local Mach number of 0.83.

For both flap settings, the approximate position of the attachment line, as indicated by the maximum C_p value, is located on the upper surface of the slat for angles of attack less than about 4 deg. Consequently, for the 40-deg flap setting and $\alpha = -1.51$ deg, the slat is shown to produce negative lift. At this negative angle-of-attack condition, lower surface flow separation is indicated by the nearly constant C_p value in the leading-edge region. On the lower surface, slat pressure ports aft of $(x/c)_{slat} = 0.30$ were actually located in the slat cove. Also in this region, the nearly constant pressure level for both flap settings at high angles of attack is indicative of flow separation in the cove. Near the lower-surface trailing edge, the pressure distributions indicate increasing flow velocities as a result of the slot flow between the slat and the main-wing element. In this region, the narrow gap for the 15-deg-flap setting caused a larger acceleration compared to the 40-deg-flap setting.

In Fig. 9, the Preston-tube measurements on the slat are plotted as a function of aircraft angle of attack for two altitudes, $h = 10$ and 20 kft, and two flap settings, $\delta_f = 15$ and 40 deg. The data show a significant increase in the measured values of C_f^* for the moderate angle-of-attack range (2.5 deg $< \alpha <$ 9.0 deg) for both flap settings, except in the lower-altitude, higher-Reynolds-number data of the 15-deg-flap setting. As mentioned earlier, at $\delta_f = 40$ deg, the flow over the slat with Preston tube starts with a new attachment point (see Figs. 4 and 5a), ensuring elimination of a turbulent inboard attachment line. This increase in C_f^* can be traced to a sudden increase in the Preston-tube total-pressure reading as opposed to its static-pressure reading that varied smoothly throughout this angle-of-attack range. This flow behavior can be related to the attachment-line boundary-layer state and the phenomenon of relaminarization and is discussed in more detail in a companion paper.[27] Briefly, if the attachment-line flow and/or the flow downstream of the attachment line become laminar as a result of changes in the pressure distribution, a significant reduction in boundary-layer thickness occurs. This reduction in boundary-layer height causes the Preston tube

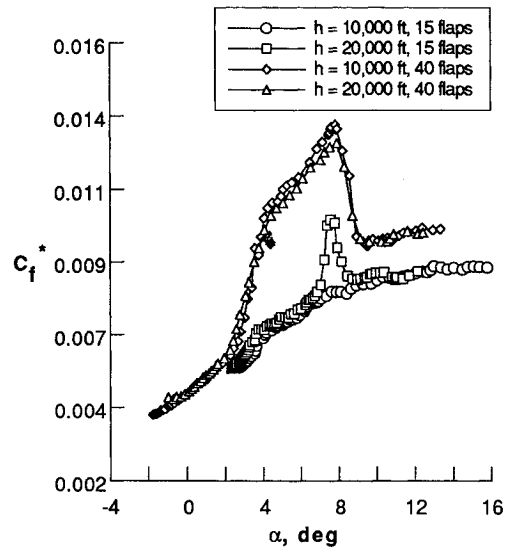

Fig. 9 Preston-tube measurements on upper surface of slat.

to be only partially submersed in the boundary layer as compared to fully submersed in the turbulent case. The outcome is an increase in the total-pressure reading of the Preston tube, and therefore, an accompanying increase in the value of C_f^*. More detailed measurements using flush-mounted static pressure orifices and hot-film sensors are planned to further study the boundary-layer transition and relaminarization phenomena on the slat.[28]

Main-Wing Element Flow Characteristics

Closer examination of the main-wing pressure distributions for the 15- and 40-deg-flap settings (Fig. 8) indicates that in both cases, there is a large suction peak at the $(x/c)_{main} = 0.12$ location of the upper surface. A local flow acceleration was registered by the pressure belt measurement at this location that corresponds to a pressure port located just behind a notch (i.e., a forward-facing step) in the leading-edge surface. The notch in the airfoil contour is a result of the slat element retracting into the main-wing leading edge for cruise flight conditions. For the 40-deg-flap case, the suction peak occurred at about $(x/c)_{main} = 0.036$, which is ahead of the notch in the surface and, consequently, a double-peaked pressure distribution is created for most of the angles of attack shown.

On the lower surface, the six most-aft pressure ports are located on the spoiler lower surface in the wing cove region. Note that the lower-surface flow apparently reattaches onto the spoiler lower surface as indicated by the high C_p value that is similar to the attachment-line value near the leading edge. The influence of the slat lower-surface, separated-flow region on the main-wing element is evidenced by the reduction in pressures in the lower-surface nose region. For the 15-deg-flap setting, the slat and main-wing elements form, in effect, a single element at lower angles of attack. The slot between the slat and the main-wing element is very narrow (see Fig. 3), causing the slat leading edge to function as the stagnation region for both the slat and the main-wing elements in low- and midrange angles of attack.

Preston-tube skin-friction measurements for the main-wing element are presented in Fig. 10 for the 15- and 40-deg-flap cases as a function of angle of attack. Three upper-surface and two lower-surface Preston tubes were attached to the main-wing element (see Figs. 4 and 5). The data indicated high values of C_f^* for probe no. 1U in the 15-deg-flap case, and for probes 1U, 2U, and 3U in the 40-deg-flap case. These high readings are indicative of the high flow velocities and thin boundary layers at those locations. Probe no. 1U is located just behind the notch in the leading-edge upper surface

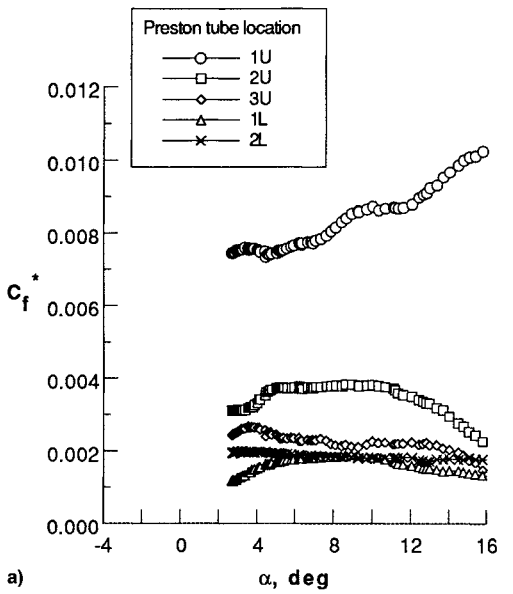

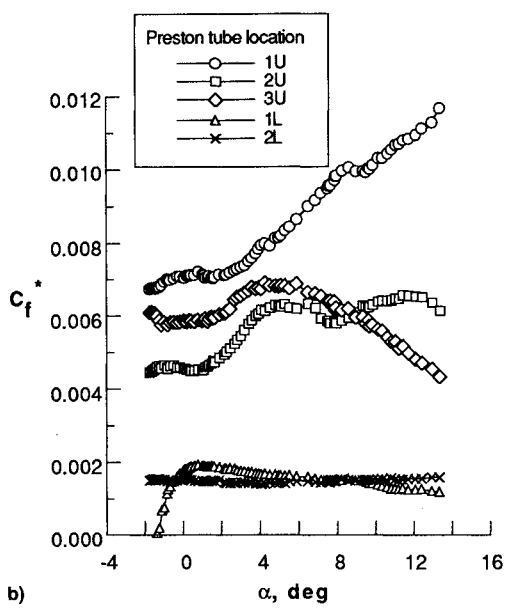

Fig. 10 Main-wing Preston-tube measurements. δ_f = a) 15 and b) 40 deg.

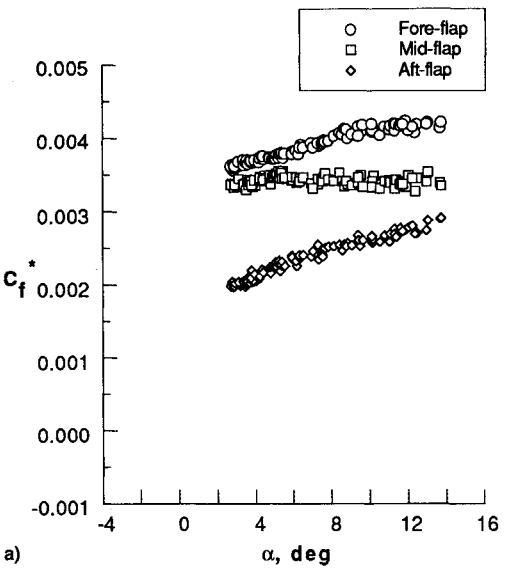

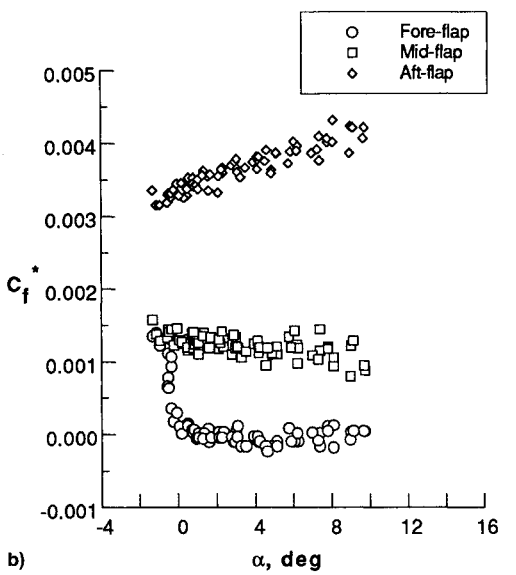

Fig. 11 Flap trailing-edge Preston-tube measurements (from Ref. 23). δ_f = a) 15 and b) 40 deg.

(see Fig. 5b). Also, in both cases, the lower-surface probe near the leading edge, probe no. 1L, experienced low C_f^* values. This result is indicative of the lower-surface slat separation bubble engulfing the main-wing leading-edge region on the lower surface. At a 40-deg-flap setting, the slat is deflected an additional amount (see Figs. 3 and 5). For the 40-deg-flap case, the C_f^* values for the midchord location, probe no. 2U, and for the aft-chord location, probe no. 3U, exhibited higher values than those for the 15-deg-flap case. This result correlates with the widening of the slat gap, which allows higher velocity flows over this region.

Flap-Elements Flow Characteristics

A detailed study of the flap pressure distributions was presented in the paper by Vijgen et al.,[23] therefore, only a limited discussion will be presented herein.

For the 15-deg-flap setting, increasing the angle of attack increased the upper-surface loading slightly, while the lower-surface pressures remained nearly unchanged (Fig. 8a). These increases in loading for the fore-flap element are small compared to the increases for the slat and main-wing elements because the in-flow angle is predominantly fixed by the geometry of the flap system. No separation is indicated in the pressure distributions for the 15-deg-flap setting, even at the highest angle of attack shown (α = 16.42 deg), although the decreasing trailing-edge pressures of the aft flap are indicative of a thickening boundary layer at higher angles of attack.

For the 40-deg-flap setting, the upper-surface loading also increased slightly with increasing angle of attack except at the highest (α = 13.38 deg) angle of attack shown (Fig. 8b). Flow separation near the trailing edge of the fore flap is indicated for all angles of attack shown except the lowest angle of attack (α = −1.51 deg). The flow separation is indicated by the nearly constant pressure level near the trailing edge upper surface of the fore flap starting at $(x/c)_{\text{fore}} \approx 0.80$. At the highest angle of attack (α = 13.38 deg), a pronounced effect of the separation on the fore flap is also observed on the midflap element.

Measurements of modified Preston-tubes located at the trailing edge of each flap element are presented in Fig. 11 to further examine the occurrence of flow separation (see Ref. 23 for Preston-tube locations on the flap). Negative values of C_f^* indicate flow separation at the Preston-tube location. For the 15-deg-flap setting, no separation is indicated for the angle-of-attack conditions measured. The higher readings for the fore flap correspond to the higher velocities associated

with the fore-flap flow. For the 40-deg-flap setting, the C_f^* values indicate separated flow on the fore flap for angles of attack greater than approximately 0 deg.

In Fig. 12, a typical flow-visualization result is shown for the 40-deg-flap setting with the aircraft operating near the stick shaker speed ($V_i \approx 105$ KIAS, $\alpha \approx 7$ deg). For this condition, the tuft patterns showed generally attached flow on the flap system, although, in the wake of the flap track fairings, localized unsteady and separated flow regions are evident. In the region of the pressure belts, the flow remained attached on the main wing and the flaps, except for flow separation near the trailing edge of the fore-flap element. The tuft patterns indicate that flow separation occurred over approximately the last 20% of the fore-flap chord. The tuft patterns correlate well with the previously discussed observations based on the pressure distributions and Preston-tube results. Figure 12 also indicates that the flow near the trailing edge of the aft flap is on the verge of separation at this condition, although the pressure distributions do not show incipient separation. Finally, the tuft patterns near the flap/aileron edge show three-dimensional tip effects in the trailing-edge region of each flap element due to the flap-edge vortical flowfield.

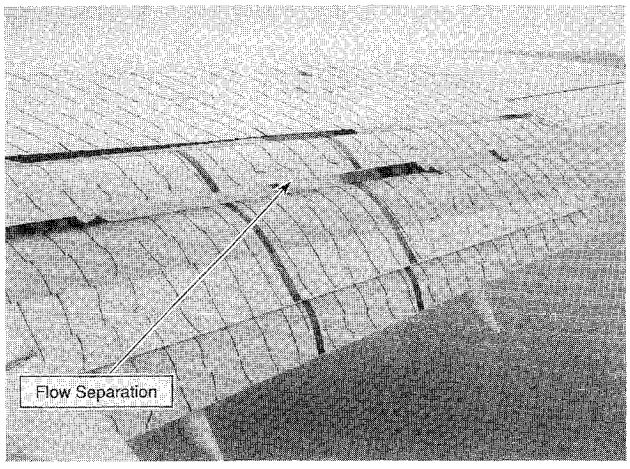

Fig. 12 In-flight flow visualization ($\delta_f = 40$ deg, $\alpha \approx 7$ deg, $V_i \approx 105$ KIAS).

Computational Analysis of Pressure Measurements

A limited computational analysis of the experimental pressure distributions at the semispan station of $\eta = 0.58$ is presented using two currently available two-dimensional computational methods. The current lack of fully three-dimensional viscous multielement analysis methods makes the use of two-dimensional methods in conjunction with appropriate sweep corrections necessary for the analysis of three-dimensional high-lift systems.[29] The sectional geometries used in the computational analysis, shown in Fig. 3, have been faired in the cove areas of the main-wing and midflap elements to facilitate the flow calculations. In the present analysis, simple-sweep

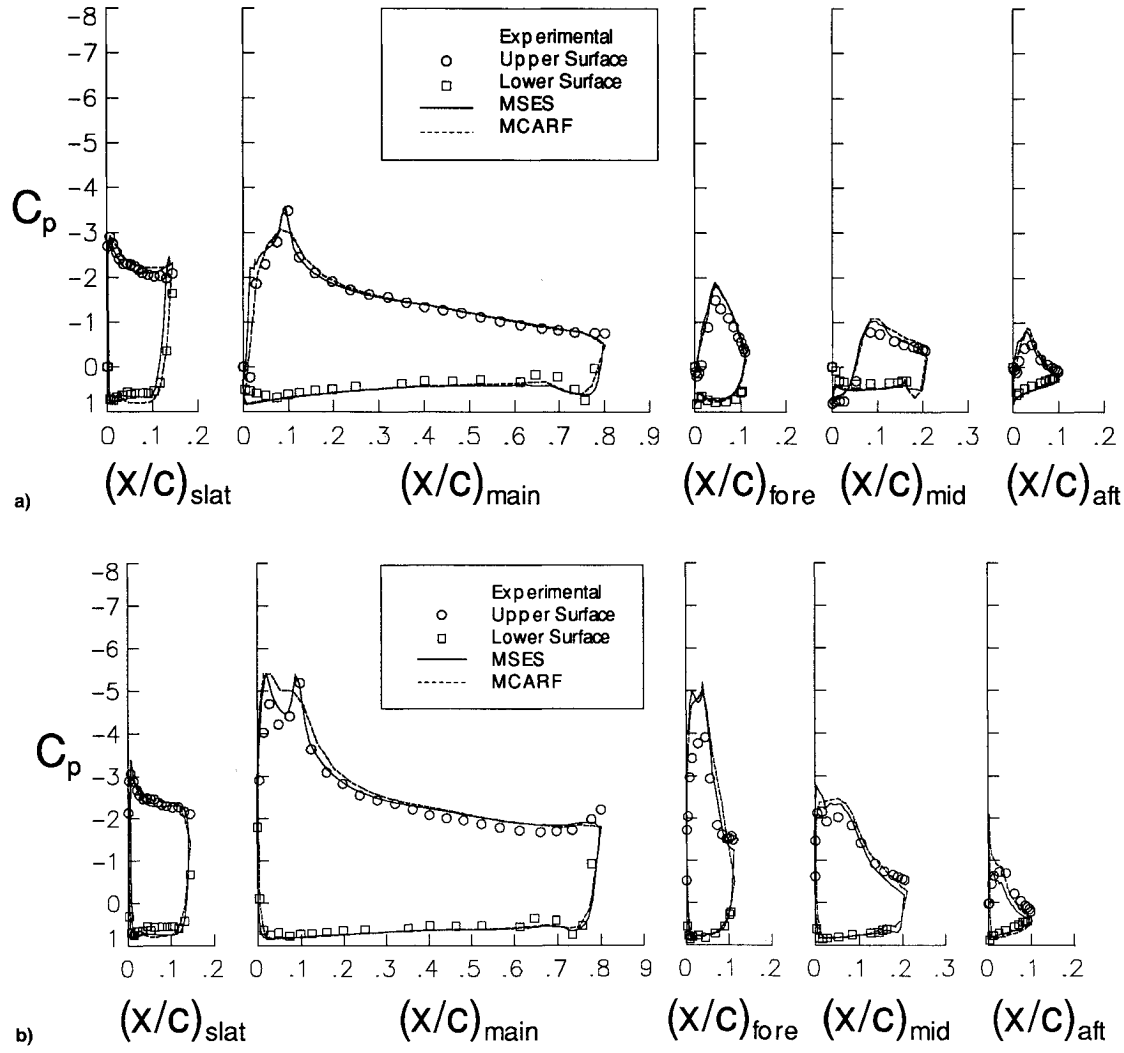

Fig. 13 Comparison of predicted pressure distributions with flight measurements: a) $\delta_f = 15$ deg, $\alpha = 9.39$ deg, $R_c = 1.47 \times 10^7$, $M = 0.24$ and b) $\delta_f = 40$ deg, $\alpha = 9.57$ deg, $R_c = 1.12 \times 10^7$, $M = 0.19$.

theory[30] is used to account for the (inviscid) sweep effects on the pressure distributions.

One of the major challenges in applying two-dimensional sectional analysis methods to three-dimensional wing geometries is the determination of the local angle of attack for input to the two-dimensional methods. For single-element wings at low angles of attack, where viscous effects are not dominant, this may be accomplished in a relatively straightforward manner by matching the predicted and experimental section normal-force coefficients. In the case of multielement high-lift systems, however, the use of the sectional normal-force coefficient is not feasible due to the strong viscous interactions, including the effects of confluent boundary layers and the presence of extensive regions of flow separation. In the results presented here, the local angle of attack was determined by matching the predicted and experimental upper-surface slat pressure distributions.

The two multielement analysis codes used are MCARF[31,32] and MSES.[33,34] In Ref. 35 comparisons are made with two-dimensional wind-tunnel data to gain insight into the prediction capabilities of the codes when compared with two-dimensional data. In this article, results of the two codes, modified for sweep effects as described previously, are compared to the flight-measured pressure distributions (Fig. 13). The comparison shows that the predicted pressure distributions are in reasonable agreement with flight-measured pressures for flap settings of 15 and 40 deg at the angles of attack shown. For the 15-deg-flap setting, where no flow separation was predicted or measured along the upper surfaces, the magnitudes of the flap element suction pressures are slightly overpredicted. However, separated flows in the lower slat-cove and along the main-wing lower-surface leading edge are not well-predicted, and the suction peak near the forward-facing step on the main-wing upper surface is not predicted in the MCARF computations. For the 40-deg-flap setting, where flow separation was measured on the fore-flap upper surface, the suction pressures over this surface are substantially overpredicted. Although the flow separation near the trailing edge is not modeled in MCARF calculations, the location of separation onset is predicted and is in agreement with the experimental separation location on the fore flap.[23] In addition, pressures are overpredicted for the leading-edge upper surfaces for all the elements aft of the slat. This overprediction of the pressures suggests that modeling of the confluent boundary layers in MCARF as well as the present approximation of three-dimensional sweep effects is not adequate for the complex high-lift geometry studied. For the 40-deg-flap setting, the MSES solution reveals small regions of flow separation near the trailing edges of the mid- and aft-flaps, as well as in the cove of the midflap. The flow over the fore flap is predicted to be separated over approximately the last 20% of the upper surface at this condition (note the nearly constant pressures in this region). This agreement in the measured and predicted flow phenomena indicates that the direct inviscid/viscous coupling incorporated in MSES allows reasonable modeling of the flow separation observed in flight.

Concluding Remarks

Flight experiments are being conducted as part of a multiphased subsonic transport high-lift research program for correlation with ground-based wind-tunnel and computational results. The NASA Langley TSRV (B737-100 aircraft) is used to obtain in-flight flow characteristics at full-scale Reynolds numbers to contribute to the understanding of two- and three-dimensional high-lift flows including leading-edge transition, confluent boundary-layer development, and flow separation characteristics.

Flight tests were performed over a range of chord Reynolds numbers from approximately 1.0×10^6 to 2.0×10^6, and freestream Mach numbers from approximately 0.16 to 0.40 for angles of attack of up to near-stall conditions. Flight test results showed that aircraft lift coefficients obtained from steady-state, trimmed conditions in level flight differed significantly from available wind-tunnel trimmed-lift coefficients due to viscous (Reynolds-number) effects. The flight-test data exhibited more linear lift curves and steeper lift-curve slopes than the wind-tunnel results. Flight test results of pressure distributions, Preston-tube skin-friction measurements, and surface-flow visualization over a full-chord wing section on a triple-slotted flap high-lift system were presented for the 15- and 40-deg-flap settings. Measurements of the pressure distributions showed that increasing the angle of attack primarily increased slat and main-wing pressure loading, but had only a small effect on the flap-element loading. For the 40-deg-flap deflection, the fore-flap upper-surface pressures indicated flow separation near the trailing edge at all but the lowest angles of attack. Tuft-flow visualization and Preston-tube results corroborated this separation on the fore-flap trailing edge. Pressure distributions for the slat and main-wing elements showed lower-surface-separation regions, reattachment locations, and aft movements of the attachment-line location with angle of attack. Pressure distributions on the slat upper surface reached high suction values that corresponded to locally high, but subsonic Mach numbers.

Preston-tube measurements on the slat outboard of the thin pressure belt indicated a likely laminar boundary-layer state at the Preston tube for certain conditions of angle of attack and altitude. Further flight experiments using hot-film instrumentation are planned to study the leading-edge transition phenomena in more detail.

A limited analysis of the experimental pressure distributions using two, two-dimensional, multielement computational codes with integral boundary-layer methods showed that the predicted pressure distributions were in reasonable agreement with flight-measured pressures for attached flow conditions. For the 40-deg-flap setting, where trailing-edge flow separation was measured over the fore flap, the pressures over the flap elements were overpredicted. This overprediction of the flap pressures suggests that current two-dimensional modeling of the confluent boundary-layer and three-dimensional (sweep) effects may not be adequate for the present, complex high-lift geometry studied. More detailed in-flight boundary-layer and flap-geometry measurements as well as the application of two- and three-dimensional Navier-Stokes analysis methods will be required to further address the effects of confluent boundary-layer development on three-dimensional high-lift systems.

Acknowledgments

The work of the second, third, and fourth author was supported under NASA Langley Contract NAS1-19299, Contract NAS1-19000, and Cooperative Agreement NCC1-163, respectively.

References

[1]Dillner, B., May, F. W., and McMasters, J. H., "Aerodynamic Issues in the Design of High-Lift Systems for Transport Aircraft," *Proceedings of the Symposium on Improvement of Aerodynamic Performance Through Boundary-Layer Control and High-Lift Systems*, AGARD CP 365, 1984, pp. 9-1–9-22.

[2]Greff, E., "In-Flight Measurement of Static Pressures and Boundary Layer State with Integrated Sensors," *Journal of Aircraft*, Vol. 28, No. 3, 1991, pp. 289–299.

[3]Brune, G. W., and McMasters, J. H., "Computational Aerodynamics Applied to High-Lift Systems," *Applied Computational Aerodynamics*, edited by P. A. Henne, Vol. 125, Progress in Astronautics and Aeronautics, AIAA, Washington, DC, 1990, pp. 389–433.

[4]Bengelink, R. L., "The Integration of CFD and Experiment: An Industry Viewpoint (Invited Paper)," AIAA Paper 88-2043, May 1988.

[5]Olson, L. E., and Orloff, K. L., "On the Structure of Turbulent Wakes and Merging Shear Layers of Multi-Element Airfoils," AIAA Paper 81-1238, June 1981.

[6]Brune, G. W., and Sikavi, D. A., "Experimental Investigation

of the Confluent Boundary Layer of a Multi-Element Low-Speed Airfoil," AIAA Paper 83-0566, Jan. 1982.

[7]Braden, J. A., Whipkey, R. R., Jones, G. S., and Lilley, D. E., "Experimental Study of the Separating Confluent Boundary-Layer," NASA CR-3655, June 1983.

[8]Nakayama, A., Kreplin, H. P., and Morgan, H. L., "Experimental Investigation of Flowfield About a Multielement Airfoil," *AIAA Journal*, Vol. 28, No. 1, 1990, pp. 14–21.

[9]Kirkpatrick, D., and Woodward, D., "Priorities for High-Lift Testing in the 1990's," AIAA Paper 90-1413, June 1990.

[10]Garner, P. L., Meredith, P. T., and Stoner, R. C., "Areas for Future CFD Development as Illustrated by Transport Aircraft Applications," AIAA Paper 91-1527, June 1991.

[11]Valarezo, W. O., Dominik, C. J., McGhee, R. H., Goodman, W. L., and Paschal, K. B., "Multi-Element Airfoil Optimization for Maximum High-Lift Reynolds Number," AIAA Paper 91-3332, Sept. 1991.

[12]Pfenninger, W., "Laminar Flow Control Laminarization, USAF and NAVY Sponsored Northrop LFC Research Between 1949 and 1967," *Special Course on Concepts for Drag Reduction*, AGARD Rept. 654, March 1977, pp. 3-1–3-75.

[13]Gaster, M., "On the Flow Along Swept Leading Edges," *The Aeronautical Quarterly*, Vol. 18, May 1967, pp. 165–184.

[14]Poll, D. I. A., "Transition in the Infinite-Swept Attachment-Line Boundary-Layer," *The Aeronautical Quarterly*, Vol. 30, Pt. 4, Nov. 1979, pp. 607–629.

[15]Launder, B. E., and Jones, W. P., "On the Prediction of Relaminarization," British Aeronautical Research Council CP-1036, Feb. 1969.

[16]Hardy, B. C., "Experimental Investigation of Attachment-Line Transition in Low-Speed High-Lift Wind-Tunnel Testing," *Proceedings of the Symposium on Fluid Dynamics of Three-Dimensional Turbulent Shear Flows and Transition*, AGARD CP 438, 1988, pp. 2-1–2-17.

[17]Arnal, D., and Juillen, J. C., "Leading-Edge Contamination and Relaminarization on a Swept Wing at Incidence," Fourth Symposium on Numerical and Physical Aspects of Aerodynamic Flows, California State Univ., Long Beach, CA, Jan. 1989.

[18]Woodward, D. S., Hardy, B. C., and Ashill, P. R., "Some Types of Scale Effect in Low-Speed High-Lift Flows," International Council of the Aeronautical Sciences Paper 4.9.3, 1988.

[19]White, J. J., "Advanced Transport Operating Systems Program," Society of Automotive Engineers Paper 901969, Oct. 1990.

[20]Montoya, L. C., and Lux, D. P., "Comparison of Wing Pressure Distribution from Flight Tests of Flush and External Orifices for Mach Numbers from 0.50 to 0.97," NASA TM X-56032, April 1975.

[21]Gracey, W., "Measurement of Aircraft Speed and Altitude," NASA RP 1046, May 1980.

[22]Bertelrud, A., "Total Head/Static Measurement of Skin Friction and Surface Pressure," *AIAA Journal*, Vol. 15, No. 3, 1977, pp. 436–438.

[23]Vijgen, P. M. H. W., Hardin, J. D., and Yip, L. P., "Flow Prediction over a Transport Multi-Element High-Lift System and Comparison with Flight Measurements," Fifth Symposium on Numerical and Physical Aspects of Aerodynamic Flows, California State Univ., Long Beach, CA, Jan. 1992.

[24]Paulson, J. W., "Wind-Tunnel Results of the Aerodynamic Characteristics of a 1/8-Scale Model of a Twin-Engine Short-Haul Transport," NASA TM X-74011, April 1977.

[25]Morgan, H. L., Ferris, J. C., and McGhee, R. J., "A Study of High-Lift Airfoils at High Reynolds Numbers in the Langley Low-Turbulence Pressure Tunnel," NASA TM 89125, July 1987.

[26]Smith, A. M. O., "High-Lift Aerodynamics," *Journal of Aircraft*, Vol. 12, No. 6, 1975, pp. 501–530.

[27]Van Dam, C. P., Vijgen, P. M. H. W., Yip, L. P., and Potter, R., "Leading-Edge Transition and Relaminarization Phenomena on a Subsonic High-Lift System," AIAA Paper 93-3140, July 1993.

[28]Yip, L. P., Vijgen, P. M. H. W., Hardin, J. D., and Van Dam, C. P., "In-Flight Pressure Distributions and Skin-Friction Measurements on a Subsonic Transport High-Lift Wing Section," *High-Lift Systems Aerodynamics*, AGARD CP 515, Sept. 1993, pp. 21-1–21-19.

[29]Brune, G. W., and McMasters, J. H., "Computational Aerodynamics Applied to High-Lift Systems," *Applied Computational Aerodynamics*, edited by P. A. Henne, Vol. 125, Progress in Astronautics and Aeronautics, AIAA, Washington, DC, 1990, pp. 389–433.

[30]Lock, R. C., "Equivalence Law Relating Three- and Two-Dimensional Pressure Distribution," British Aeronautical Research Council R&M 3346, May 1962.

[31]Stevens, W. A., Goradia, S. H., and Braden, J. A., "Mathematical Model for Two-Dimensional Multi-Component Airfoils in Viscous Flows," NASA CR-1843, July 1971.

[32]Brune, G. W., and Manke, J. W., "An Improved Version of the NASA-Lockheed Multielement Airfoil Analysis Computer Program," NASA CR-145323, March 1978.

[33]Drela, M., "Newton Solution of Coupled Viscous/Inviscid Multi-Element Airfoil Flows," AIAA Paper 90-1470, June 1990.

[34]Drela, M., "A User's Guide to MSES V1.2," Massachusett's Inst. of Technology Computational Fluid Dynamics Lab., Cambridge, MA, July 1991.

[35]Hardin, J. D., Potter, R. C., Van Dam, C. P., and Yip, L. P., "Two-Dimensional Computational Analysis of a Transport High-Lift System and Comparison with Flight-Test Results," AIAA Paper 93-3533, Aug. 1993.